ORIGINAL PAPER

New magnetic/Biosilica/Sodium Alginate Composites for removal of Pb (II) ions from aqueous solutions: kinetic and isotherm studies

Mehdi Hosseini[1, 2], Ali Esrafili[1, 2], Mojtaba Yegane badi[1, 2], Mitra Gholami[1, 2, ✉]

1. Research Center for Environmental Health Technology, Iran University of Medical Sciences, Iran
2. Department of Environmental Health Engineering, School of Health, Iran University of Medical Sciences, Tehran, Iran

Date of submission: 11 Apr 2018, ***Date of acceptance:*** 12 Aug 2018

ABSTRACT

Lead is one of the heavy metals that have harmful effects on the human health and environment. In this study, a new magnetic/biosilica/sodium alginate adsorbent (MBSA) made by the coprecipitation method was used to remove lead from aqueous solutions. It was an experimental study conducted at laboratory scale. The properties of MBSA were analyzed by scanning electron microscope (SEM), XRD, and FTIR analyses. The influences of various parameters such as contact time (0–80 min), pH (3–11), initial lead concentration (10–80 mg/L), temperature (298–318 ºK), and adsorbent dosage (0.5–4 g/L) on the sorption process were investigated. The equilibrium isotherm and kinetic models were used to evaluate the fitness of the experimental data. The results showed that lead removal using MBSA was obtained at an optimum pH of 11, contact time of 80 minutes, adsorbent dosage of 4 g/L, lead concentration of 10 mg/L (46.29 g/g), and temperature of 318 ºK. Investigating the isotherm and kinetic equations showed that the experimental data of the lead adsorption process correlate with the Langmuir model (R^2 = 973) and intraparticle diffusion kinetic model, respectively. The values of the thermodynamic parameters (ΔH°, ΔG°, ΔS°) indicated that the sorption of Pb (II) ions on MBSA was spontaneous and endothermic in nature. Due to the good removal efficiency, low cost of the process, and lack of production of harmful substances for the environment, this adsorbent can be used to remove lead from the industrial wastewater.

Keywords: Adsorption, MBSA, Adsorbent, Aqueous solution, Heavy metals

Introduction

In recent years, due to the activity of various industries such as metal plating, oil and gas refineries, color industries, printing, building batteries, plastics, etc., heavy metals have entered into the environment, especially the water sources, in large quantities and over the permissible limit.[1-4] Because heavy metals are not biodegradable, they can remain in the environment and accumulate in organisms and enter the food chain.[5] The entry of these substances into the human body causes undesirable health effects, including cancer, effects on the kidneys, liver, central and peripheral nervous systems, and reproduction.[6,7]

Lead is one of the heavy metals that can be introduced into the water resources due to industrial activities. The maximum permissible level of this metal in drinking water according to the US Environmental Protection Agency is 0.1 mg/L.[8] Like other heavy metals, lead also has harmful effects on human health. Due to the accumulation of this substance in the body, diseases such as anemia, encephalopathy, hepatitis, and nephrotic syndrome can occur.[1,7,9,10] Hence, the removal of this metal from industrial wastewater and water resources is essential.

Different methods have been used to remove lead and heavy metals from aqueous solutions such as ion exchange, membrane filtration,[11] photoelectric precipitation,[12] coagulation, chemical precipitation, and adsorption in various studies.[6-13] Among these methods, the adsorption process has special advantages such as low cost, ease of use, easy

✉ *Mitra Gholami*
gholamimitra32@gmail.com

Citation: Hosseini M, Esrafili A, Yegane badi M, Gholami M. New magnetic/Biosilica/Sodium Alginate Composites for removal of Pb (II) ions from aqueous solutions: kinetic and isotherm studies. J Adv Environ Health Res 2018; 6(3): 160-172

operation, high flexibility, and insensitivity to toxic contaminants.[14,15] So far, many adsorbents have been used to remove heavy metals.[16,17] But, some of these adsorbents have low surface area and limited adsorption capacity, and subsequently, low adsorption efficiency; many nanosized adsorbents have been limited by some problems such as filtration, centrifugation, and occurrence of turbidity in the effluent. Therefore, the use of adsorbents which show a rapid and simple separation and do not cause secondary pollution should be considered. However, natural adsorbents are considered very efficient. These adsorbents do not have the disadvantages of the synthetic adsorbents, such as high production cost and regeneration.[18] Alginate, a type of hydrogel, is one of the most widely used adsorbents in the removal of various contaminants due to its non-toxicity, environmental friendliness, and low cost.[19] The adsorbent has hydroxyl groups (-OH), carboxyl (-COOOH), (NH_2^-), and (OSO_3) which convert it into a suitable adsorbent for heavy metals.[20] However, this biopolymer requires physicochemical modification due to decomposition, swelling, and low mechanical stability in water.[19,21] In many publications, siliceous and clay soils have been used to reduce material swelling and improve its mechanical stability.[13-19] Among the existing soils, diatomite, which is a silicon sedimentary rock, due to its physical and chemical properties such as high porosity, high surface area, light weight, and high adsorption properties has attracted much attention in eliminating the defects of hydrogels.[22-24] Magnetic nanoparticles are the other adsorbents used to remove heavy metals.[25] These materials have a high surface area, nanosize, and high performance, and their synthesis requires low cost.[10] The disadvantages of these nanomaterials are their agglomeration in aquatic environments (which reduces their surface area),[26-27] and entry into water resources and their associated risks for human and environmental health. To overcome these problems, they can be combined in heterogeneous systems coupled with hydrogel.[10] Combining the nanomagnets with hydrogel systems, in addition to eliminating the defects of the nanostructures, increases the hydrogel's performance and the magnetic property of the hydrogel in the composition and provides the ability to separate the adsorbent from the aqueous environments using an external magnet.[1] However, the removal of Pb^{2+} using magnetic/biosilica/sodium alginate composites as adsorbent has not been reported in the literature. One of the advantages of magnetic/biosilica/sodium alginate composites is that it can be employed in situ, and thus, is suitable for online separation. In this study, a new compound absorbent sodium alginate/diatomite/magnetic was used to remove lead from aqueous solutions. The effect of the different factors such as contact time, pH, temperature, the initial concentration of lead, and the adsorbent dosage on the efficiency of removal of lead by the adsorbent was investigated.

Materials and Methods

Chemicals

In this research, materials such as lead nitrate, sodium hydroxide, hydrochloric acid, acetic acid, ferric chloride 6 hydrate ($FeCl_3.6H_2O$), iron sulfate 7 hydrate ($FeSO_4.7H_2O$), sodium triphosphate, ammonia solution, and sodium alginate were purchased from Merck Co. (Germany), and diatomite was obtained from Sigma Aldrich (USA). Ionized water was used in all experiments for solubilization. A stock solution of Pb^{2+} (1000 mg/L) was prepared by dissolving the required amount of lead nitrate ($Pb(NO_3)_2$) in distilled water. Subsequently, the remaining Pb^{2+} concentrations in the samples were evaluated using atomic absorption spectrophotometry (AAS, Analyst 200) at a wavelength of 283.3 nm. The lamp current and slit width was 13 mA and 0.5 nm, respectively. All measurements were performed in an air/acetylene flame.

Preparation of adsorbent

Preparation of magnetic nanoparticles

Coprecipitation method was used to make magnetic nanoparticles. In this method, $FeSO_4.7H_2O$ and $FeCL_3.6H_2O$ (1:1) were dissolved in 0.3 molar concentration in

deionized water. The mixture was stirred under nitrogen gas at 80 ºC for 30 min. Then, the ammonia mixture with a purity of 25% was added at pH 10 and then again under nitrogen gas for one hour. The magnetic nanoparticles were separated from the reaction solution using a magnet and washed several times using ethanol and water. The dispersed nanoparticles were dried at 70 ºC for 24 hr.[28]

Preparation of MBAS

To prepare the nanocomposite, first, 1 g of sodium alginate was added to 100 mL of acetic acid (1 M) solution and mixed for 2 hr. Then, 1 g of biosilica and 1 g of magnetic nanoparticles were added to the solution and stirred to reach a uniform viscosity mixture. The resulting mixture was placed under completely residual conditions for 10 hr to remove all the bubbles from the solution and obtain a bubble-less mixture. Then, 100 mL of the mixture in a ratio of 4:1 of 15% NaOH and 95% ethanol was prepared, and a viscose mixture of sodium alginate/biosilica/magnetic alginate was added to the mixture of NaOH and ethanol using a drop of droplets and stored for 24 hr in the above solution until pelletized beads were formed. Then, the resulting beads were washed with distilled water (until neutral pH was reached) and dried at ambient temperature to reach a constant weight. Finally, the dried mixture was chopped and meshed using sieves.[29]

Characterizations and analysis

The surface morphology and elemental composition of the MBSA were determined using a scanning electron microscope (SEM, Jeol ModelJsm-T330) equipped with an X-ray energy spectroscopy (EDX) under stable vacuum. The Fourier Infrared Conversion Facility (FTIR) (JASCO, FT / IR-6300Japan) with a 1 cm^{-1} diaphragm reflectance technique in a range of 400–4000 cm to determine the MBSA functional groups involved in the adsorption process. An X-ray analysis (X-ray diffraction) was performed on an XPERT-PRO diffractometer using PW3050/60 (Theta/Theta) Protractor to investigate the particle size and structural properties. Diffraction images with a 2-degree angle θ with a start and end position were recorded at 10 and 80 degrees, respectively, at a speed of one second. After obtaining the corresponding images, the particle size was calculated using the Debye-Scherrer relation given in Equation 1:[30]

$$D=\frac{K\lambda}{\beta cos\theta} \quad (1)$$

Where K is a constant equal to 0.89, λ is the X-ray wavelength equal to 0.154056 nm, β is the line broadening at half the maximum intensity in radians, and θ is the Bragg angle in degrees. To determine the pH at the zero point charge (pH_{ZPC}) of the adsorbent, 50 mL of NaCl solution (0.01 M) was added to six Erlenmeyer Flask of 100 mL volume, and its pH was adjusted to between 2 and 12 (initial pH). Then, 0.5 g of the adsorbent was added to each of the above solutions and placed on a shaker at 200 rpm for 24 hours. Next, the adsorbent was separated from the solution, and the pH of the solution (secondary pH) was measured. pH_{ZPC} was obtained by plotting the initial pH versus the secondary pH and their intersection.[31]

Adsorption analysis

In this study, a batch system was used to identify the effect of the different parameters including contact time (0–80 min), initial concentration of lead (10–80 mg/L), pH (3–11), temperature (298–318 ºK), and adsorbent dosage (0.5–4 g/l) on the adsorption of lead using MBSA adsorbent. A 3 Tesla magnet was used to remove the adsorbent from the solution. The sorption experiments were conducted in duplicates, and the average concentrations were considered. The removal rate of lead was calculated using Equation 2:

$$Removal\ rate=\frac{C_{in}-C_{out}}{C_{in}}\times 100 \quad (2)$$

Where C_{in} and C_{out} are the lead concentrations before and after adsorption, respectively. The uptake capacities of the sorbent were computed by Equation 3.[32]

$$qe=\frac{(C_0-Ce)V}{m} \quad (3)$$

Where qe (mg/g) is the equilibrium uptake

capacity of lead on the adsorbent, C_0 and C_e is the initial and equilibrium concentration of lead (mg/L), respectively, m (g) is the adsorbent mass, and V (L) is the volume of solution.

Adsorption isotherm

One of the most important ways to study the interactive behavior, adsorption surface properties and adsorption mechanisms, between the adsorbent and adsorbed is to survey the adsorption isotherm.[33, 34] In this study, three most commonly isotherm models, Langmuir, Freundlich, and Dubinin- Radushkevich (D-R) isotherm models, were used to study the adsorption isotherm. The linear model of the adsorption isotherm is given below.

$$\frac{C_e}{q_e}=\frac{C_e}{Q_m}+\frac{1}{bQ_m} \quad (4)$$

The above equation, which is the Langmuir model, has the following parameters: Ce (mg/L) is the concentration of lead in solution at equilibrium time, qe (mg/g) is the sorption capacity at equilibrium time, b is the Langmuir constant (L/mg), and Q_m (mg/g) is the maximum adsorption capacity. Q_m and b are determined from the gradient and intercept obtained by plotting C_e/q_e against C_e, respectively.[35] One of the parameters of the Langmuir equation is the separation coefficient (R_L). This coefficient determines the type of adsorption process, and its equation is as follows:

$$RL=\frac{1}{(1+bC_o)} \quad (5)$$

Where RL is the separation coefficient, and Co is the initial concentration (mg/L). If $R_L = 0$ is the irreversible adsorption process, $0 < R_L < 1$ is the desirable process, RL = 1 linear process, and $R_L > 1$ will be considered undesirable process.[36]

The Freundlich model is based on single-layer adsorption on heterogeneous adsorption sites. It should be noted that this model is not exclusive to single-layer adsorption and is also used for multi-layer absorption.[37] The linear model of the Freundlich isotherm model is given by Equation 6.

$$lnq_e=ln\ k_f+\frac{1}{n}ln\ C_e \quad (6)$$

In this equation, k_f (L/g) and n are the constants of the equation. Log_{kf} is the intercept of the Freundlich model, an index of adsorption capacity, and 1/n, the slope of the Freundlich model line, is an indicator of adsorption intensity.[38]

Isotherm (D-R) is used to determine the thermodynamic properties of adsorption and is based on heterogeneous surfaces.[39] The linear form of its equation is given in Equation 7.

$$ln\ q_e = ln\ q_m - \beta\ \varepsilon^2 \quad (7)$$

Where β (kJ/mol) is a constant energy-related parameter, and Ɛ (Polanyi potential) is dependent on the equilibrium obtained by the following equation.[40]

$$\varepsilon = RT\ ln\left(1+\frac{1}{C_e}\right) \quad (8)$$

In this relation, R (kJ/mol. K) is the gas constant, and T is the temperature in ºk. qm and ß are calculated in Equation 7 through the intercept and gradient of the ln qe curve versus $Ɛ^2$. E (kJ/mol), the free energy of adsorption, is calculated by Equation 9.

$$E=\frac{1}{\sqrt{2\beta}} \quad (9)$$

The amount of E represents the type of physical or chemical adsorption process. E < 8 kJ/mol and E > 16 kJ/mol indicate physical and chemical adsorptions, respectively, and the E value between 8 and 16 kJ/mol represents the chemical ion exchange in the solution.[41]

Adsorption kinetic

Pseudo-first-order, pseudo-second-order, and intraparticle diffusion models were used to investigate the mechanism of the process controller and determine the rate of the adsorption process. The pseudo-first-order model is based on Equation 10:

$$ln\left(q_e-q_t\right)=ln\ q_e-k_1 t \quad (10)$$

Where q_e (mg/g) and q_t (mg/g) are the amount of lead adsorbed on MBSA at equilibrium time and time t, respectively. k_1

(L/min) is the rate constant of the pseudo-first-order model. The values of q_e and K_1 are obtained from the intercept and gradient of the line from the drawing of ln (q_e-q_t) versus t.[42] The pseudo-second-order model is in accordance with Equation 11:

$$\frac{t}{q_t} = \frac{1}{k_2 q_e^2} + \frac{t}{q_e} \quad (11)$$

Where q_e (mg/g) and q_t (mg/g) are the same parameters expressed in the pseudo-first-order equation. k_1 (L/min), the constant rate of pseudo-second-order model, and q_e are obtained through the gradient and intercept of the line from drawing t/q_t vs. t.[31] The mathematical expression of the intraparticle diffusion kinetic model is as follows:

$$q_t = k_{id} t^{0.5} + C \quad (12)$$

Where K_{id} (g/mg.min) is the rate constant of the intraparticle diffusion model, C is the constant of the intraparticle diffusion model in mg/g, and q_t is the adsorption capacity at time t. By drawing qt against $t^{0.5}$, the values of k_{id} and C are obtained from the intercept and slope of the line, respectively.[43]

Effect of temperature and thermodynamic studies

The adsorption of lead by MBAS was specified in the temperature range 298–318 ºK. The thermodynamic parameters in this study were calculated using Equations 13 and 14:

$$\Delta G = -RTLnk \quad (13)$$

$$K = \frac{q_e}{C_e} \quad (14)$$

$$\Delta G = \Delta H - T\Delta S \quad (15)$$

$$Lnk = \frac{\Delta S}{R} - \frac{\Delta H}{RT} \quad (16)$$

Where, k (L/g) is the standard thermodynamic equilibrium constant, R (8.314 J/mol K) is the gas constant, and T (ºK) is the absolute temperature. The values of enthalpy (ΔH kJ/mol) and entropy (ΔSJ/K mol) were obtained from the intercept and slope of plotting ln k against 1/T in Equation 16, respectively.[44]

Results and Discussion

Characterization of the MBAS

The surface morphology of MBSA, sodium alginate, biosilica, and magnetic as depicted by the scanning electron microscopy is shown in Fig. 1 (a), (b), (c), and (d), respectively. As shown in the figure, the porosity of the image (d) of the MBSA is much higher than the other adsorbents shown. The elemental analysis of the adsorbent composition presented in Fig. 2 shows the presence of iron, silica, sodium, oxygen, and aluminum. Based on the results of the elemental analysis of the adsorbent, it can be concluded that the oxidation of iron nanoparticles by acid used to prepare the adsorbent is inhibited by silica.[20] Moreover, these findings indicate the proper composition of the materials used to make MBAS.

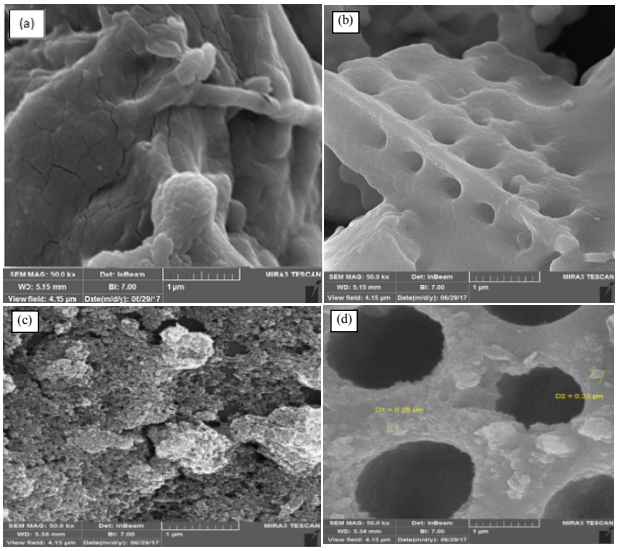

Fig. 1. SEM images of the (a) sodiumalginate, (b) biosilica, (c) magnetic, (d) MBAS

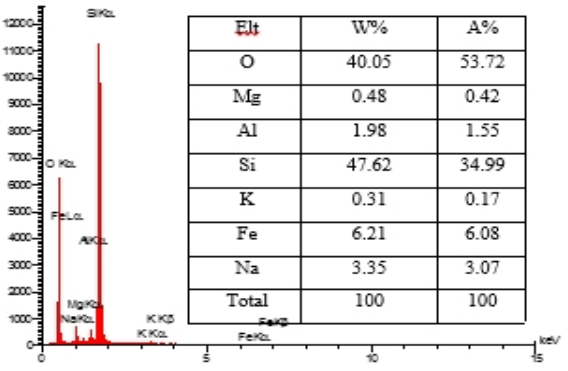

Elt	W%	A%
O	40.05	53.72
Mg	0.48	0.42
Al	1.98	1.55
Si	47.62	34.99
K	0.31	0.17
Fe	6.21	6.08
Na	3.35	3.07
Total	100	100

Fig. 2. SEM–EDX analytical results of MBAS

Fig. 3 displays the XRD pattern of MBSA, nanomagnets, biosilica, and alginate. In the magnetic pattern, the deflected peaks at the angle 2θ of 30.6, 36.04, 43.6, 54.2, 57.6, and 63.25 are related to the crystalline plates 220, 311, 400, 422, 511, and 440, respectively, which correspond to the Fe_3O_4 cubic phase (JCPDS card No. 19-0629).[17] Also, the peak mentioned in the MBSA pattern indicates that Fe_3O_4 is present in the MBSA compound. As shown in Fig. 3, the peaks obtained for biosilica are in accordance with the pure silica phase (JCPDS ICDD File Card # 00-001-0647) and are quite obvious in the MBSA pattern.[29] The peaks present at 13.5 ° and 22.1 ° are related to sodium alginate, which is visible in the alginate pattern and MBSA. The mentioned angles are due to the reflection of the plates 110 and 200 that correspond to polyguluronate and polymannuronate units, respectively.[45] As shown in Fig. 3, the intensity and sharpness of the peaks in the composite are reduced in comparison with Fe_3O_4 and biosilica, which can be related to their composition with alginate because the alginates have an amorphous nature and can affect the general pattern of MBSA.

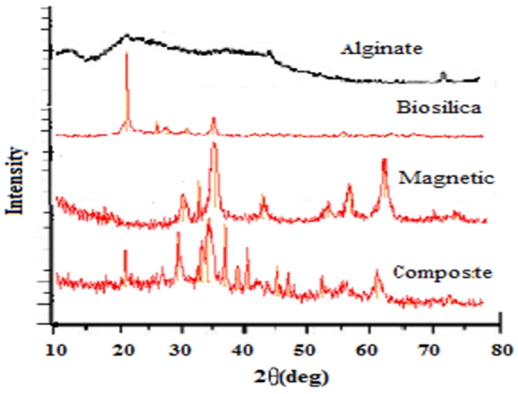

Fig. 3. XRD pattern of sodium alginate, biosilica, magnetic, and MBAS

The FTIR spectrum of sodium alginate, magnetic, biosilica, and MBSA before and after lead adsorption is displayed in Fig. 4. The hydroxyl and ester groups, carboxylic acid, mannuronic acid, and uronic acid are seen in the alginate spectrum.[46,47] The bands at 1626 and 1453 cm^{-1} are related to the asymmetric and symmetric stretching vibration of carboxylate anions (COO-), respectively. Because of the polysaccharide property of the alginate, the peak at 1093 cm^{-1} (C-O-C asymmetric stretching) and 866 and 906 cm^{-1} (C-O-C symmetric stretching) are also visible within the corresponding spectrum.[48] A strong and broad band at 3442 cm^{-1} that relates to the stretching vibrations of the O-H groups and the peak at 2924.67 cm^{-1} that corresponds to a poorly aliphatic bond of stretching vibration of the C-H are seen in the alginate spectrum. In the biosilica spectrum, peaks in the region of 3200–3700 cm^{-1} represent the stretching vibration of Si-OH. The band at 1630 represents the H-O-H bond vibration; the bands at 1095, 793, and 472 cm^{-1} are assigned to the stretching vibration of the siloxane group (Si-O-Si).[49,50] As it is known in the magnetic spectrum, four major peaks are noteworthy. The 3450 cm^{-1} band, as previously mentioned, refers to the stretching vibrations of the OH groups and the peaks at 635, 582, and 474 cm^{-1}, all of which are related to the Fe-O vibrating bonds.[17-28] On comparing the two peaks of the adsorbent before and after the adsorption of lead, it can be seen that the peaks located at regions 3422, 2924, 2366, 1627, 1453, 1093, 793, 635, and 474 cm^{-1} after the adsorption of lead on the adsorbent are broad, and the percentage of transfer to them declined, which indicates the impact of the functional groups associated with the situations mentioned in the adsorption process.

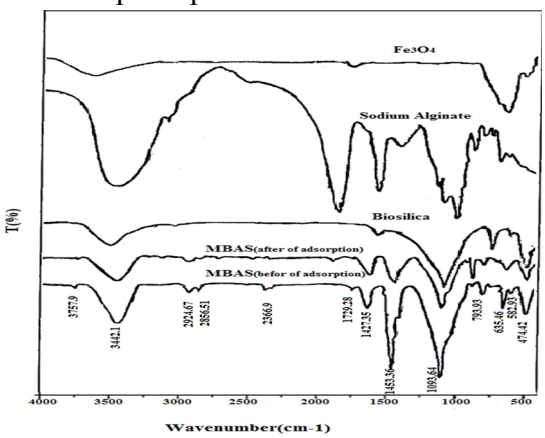

Fig. 4. FTIR spectra of sodium alginate, biosilica, magnetic, and MBAS

pHpzc of adsorbent and effect of pH

One of the important parameters that

determine the mechanism of adsorption process is the pH_{ZPC} of the adsorbent. Figure 5 (b) shows the pH_{ZPC} of the MBAS. The pH_{ZPC} of the adsorbent was 9.6, which causes the adsorption surface to have a positive charge below this value and a negative surface charge at higher pH. This indicates a high dependence of the adsorption capacity on the pH of the solution.[51] Fig. 5a shows the effect of the initial pH of the solution on the removal of lead from the aqueous solution. As can be seen, with the increase in pH, the removal of lead increases. The result is consistent with the results for pH_{ZPC} because, as mentioned, it is expected that to have a negative adsorbent surface charge at pH values higher than 9.6, and since the charge of lead is positive, it leads to better adsorption of lead at higher levels onto the adsorbent surface. Farooghi et al. found that the removal percentage can be reduced by reducing the pH in the presence of H^+ ions at low pH values when these ions are in competition with lead metal that has a positive charge on the occupancy of the adsorbent active sites and reduce the available sites for lead adsorption on the adsorbent surface.[25,52,53] In the study done on the removal of lead using iron oxide modified with sericite alginate grains, with increasing pH, the adsorption of lead increased.[1]

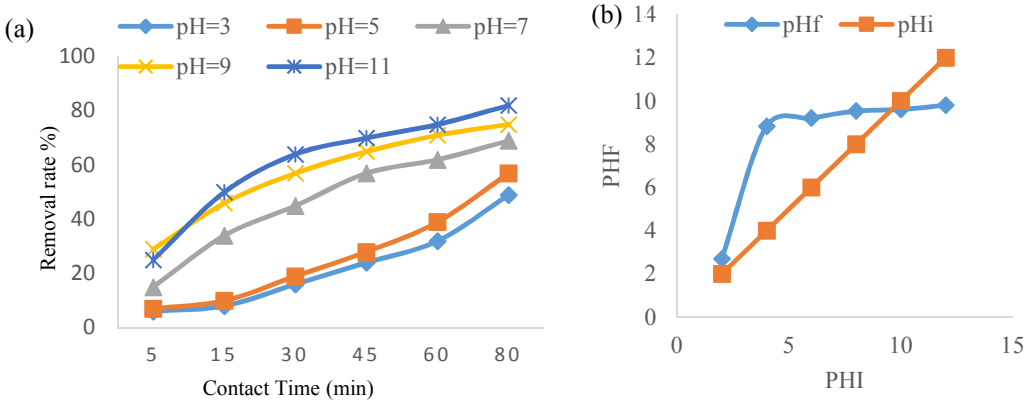

Fig. 5. (a) The effect of solution pH on the adsorption of lead by the MBAS (lead solution = 10 mg/L min, 318 ºK, and adsorbent conc. = 0.5 g/L) and (b) pH_{zpc} of the sorbent

Effect of initial concentration

The results of the lead adsorption experiments at various initial concentrations of lead are shown in Fig. 6. As shown in the figure, on increasing the concentration of the pollutant to 30 mg/L, the removal percentage increased with a steep slope and then decreased with a less steep slope. This was probably due to the constant of the adsorbent active sites in a constant dose of MBAS, so these sites occupied by a certain concentration of the contaminant and higher cannot adsorb on to the adsorbent. Furthermore, the reason for the very low reduction in the removal percentage at higher concentrations can be attributed to the desorption of the adsorbed metal into the solution.[54] Ghaemi et al. found that increasing the initial concentration of lead reduced its adsorption.[7] In a study on lead and copper adsorption using sodium alginate, on increasing the initial concentration of lead and copper until a certain amount, the removal percent increased and then remained constant.[55]

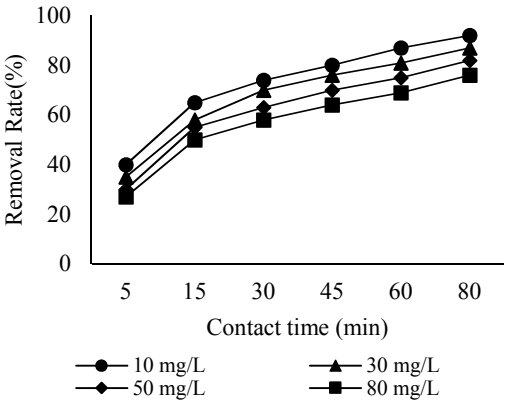

Fig. 6. The effects of lead concentration on the adsorption by MBAS (pH =11, 318 ºK, and adsorbent conc.= 0.5 g/L)

Effect of adsorbent dosage

The effect of the adsorbent on the removal rate of lead was studied using different adsorbent dosages (0.5–4 mg/L). Based on the results shown in Fig. 7, lead removal increased significantly with increase in the adsorbent dosage. The percentage of lead removal with 0.5 g/L of adsorbent was 82% at 80 minutes while this value was 92% at the same time for 4 g/L of adsorbent dosage. When a solid surface of adsorbent comes in contact with the noxious metal ion, rapid removal of ions from the aqueous solution occurs.[56,57] Increasing adsorption by increasing the amount of the adsorbent is the result of an increase in effective levels, functional groups, and sites available for the adsorbent substance.[58] Another reason for the increased removal rate could be the increase in the collision between the pollutant and adsorbent molecules and, consequently, the increase in the gradient concentration and mass transfer.[59] The results of this study are consistent with the results of the study by Shi et al. and Vijayalakshmi et al. on the removal of chromium (II) using bentonite coated with iron,[60] and eliminating lead using nanocytosine /sodium alginate/microcrystalline cellulose.[61] The resultant removal efficiency is in line with that reported by Acharya et al. wherein the removal efficiency ranged from 86.6% to 96% when commercially activated carbon was applied in the dosage range 1 to 5 mg/L, respectively.[62]

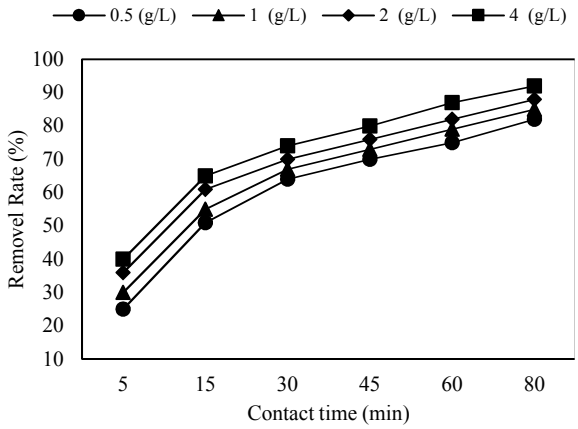

Fig. 7. Effect of adsorbent dosage on the sorption capacity (lead concentration=10 mg/L, 318 ºK, pH=11)

Table1. Langmuir, Freundlich and D-R isotherm parameters for the adsorption of lead by MBAS

Langmuir isotherm			Freundlich isotherm			D-R isotherm		
R^2	b (L/mg)	Q_m (mg/g)	R^2	n	K_f	R^2	E (kJ/mol)	q_m (mg/g)
0.973	0.96	46.29	0.939	1.37	0.252	0.943	0.585	8.88

Effect of contact time

The effect of contact time on the amount of lead adsorption is shown in Fig. 7. As shown in the figure, the percentage of removal increased with increasing contact time for all concentrations. Between 5 to 15-minute time ranges, the lead with a sharper slope was eliminated from the reaction solution. At other times, the removal percentage gradually increased with a steady slope. In a study by Kakavandi et al. (Pb (II) adsorption on a magnetic composite of activated carbon and superparamagnetic Fe_3O_4 nanoparticles), the authors concluded that with increasing contact time, the removal efficiency increases.[8]

Adsorption isotherm

The parameters of the three isotherms used in the lead adsorption process on MBSA are given in Table (1). The most suitable isotherm model in this study was the Langmuir isotherm (R^2 = 0.97), which shows the adsorption of a single-layer of lead in special homogeneous locations on the adsorbent outer surface that stopped after reaching the saturation state during the equilibrium of the adsorption process.[63,64] Based on the amount of RL obtained in this study (0.012), the adsorption process used was desirable. The Langmuir isotherm is shown in Fig. 6 (b). Various studies have also suggested Langmuir isotherm as the most appropriate isotherm model for adsorbing heavy metals using various adsorbents.[27,65]

Adsorption kinetic

The results of the analysis of the different kinetic models of lead adsorption on MBSA are presented in Table 2. As shown in the table, the

intraparticle diffusion kinetic model is more suitable for the adsorption process used in this study ($R^2 = 0.993$). In Fig. 7 (b), the intraparticle diffusion kinetic model is shown. In addition, the pseudo-first-order kinetic model with a correlation coefficient of 0.992 can also be a suitable model for the process. Also, the calculated adsorption capacity (q_e, calculated) in the pseudo-first-order kinetic model is approximately the same as the adsorption capacity of the experiments (q_e, experimental), which is another reason for the suitability of this model in the adsorption of lead on MBSA. Based on the findings of the first-order kinetic model, it can be stated that adsorption has only occurred on topical sites, and the removal rate of lead is proportional to the number of sites active in the adsorbent, and the adsorption energy does not depend on surface coating.[7] With respect to the intraparticle diffusion theory and the high correlation coefficient obtained in this study, it is argued that after adsorption of lead on the adsorbent surface, its diffusion is carried out into the porous adsorbent, and the adsorption mechanism is complete.[42] Since the correlation coefficient obtained for the pseudo-second-order model was close to the other two models, it can be concluded that lead absorption also partly confirms the chemical absorption mechanism. Woo et al. found that the pseudo-first-order kinetic model is a suitable model for chromium adsorption on iron sulfide nanoparticles coated on the surface of sodium alginate.[66] Vorma et al. reported the proper model in the glycine-induced adsorption process of magnetic nanoparticles coated on sodium alginate to be pseudo-second-order; however, they considered two first-order kinetic models and intraparticle diffusion model weakly involved in the adsorption kinetic.[10]

Table 2. Parameters of various kinetic models for the adsorption of lead by MBAS

	Pseudo-first order			Pseudo-second order			Intra-particle diffusion		
$q_{e,\ Experimental}$	R^2	k_1	$q_{e,\ Calculated}$ (mg/g)	R^2	k_2	$q_{e,\ Calculated}$ (mg/g)	R^2	C	k
11.36	10.83	0.029	0.992	14.7	0.002	0.981	1.37	0.979	0.993

Effect of temperature and thermodynamic studies

The thermodynamic parameters of lead adsorption on MBAS are listed in Table 3. As represented in Table 3, the values of ΔH and ΔS were positive, and the standard free energy (ΔG) was negative. The positive ΔH value indicates that the sorption process was endothermic. In other words, the positivity of this parameter states that the increase in temperature has a positive effect on the adsorption of lead and, the adsorption of this pollutant at higher temperatures is more favorable. Furthermore, the negative values obtained for Gibbs free energy indicate that the adsorption of lead by the synthesized adsorbent is a spontaneous process.[67]

Table 3. Thermodynamic parameters for the adsorption of lead ion on MBAS

Thermodynamic parameters				
Temperature (°K)	ln K_D	ΔG° (kJ/mol)	ΔH° (kJ/mol)	ΔS° (kJ/mol.K)
298	1.81	-4.490		
308	2.05	-5.185	107.163	0.2628
318	3.19	-8.323		

Conclusion

In this study, a new magnetic/biosilica/sodium alginate adsorbent made using the coprecipitation method was used to remove lead from aqueous solutions. The effect of the different parameters on lead elimination, such as the initial pH, adsorbent dosage, initial lead concentration, and contact time, were investigated. The results of this study showed that the most suitable pH for the removal of lead from the reaction solution was 11, and by increasing the adsorbent dosage and

reducing the initial pollutant concentration, the removal rate could be increased. The achieved equilibrium time in this study was 80 minutes, with a maximum adsorption capacity of 46.27 mg/g. The kinetic model of intraparticle diffusion model and Langmuir isotherm were the most suitable kinetic and isotherm models to describe the speed and mechanism of the adsorption process. Thermodynamic studies were also conducted, and the outcomes suggested the spontaneous and endothermic nature of Pb (II) ions sorption on MBSA. It seems that the magnetization of adsorbents and use of magnetic separation techniques can be an effective way to resolve the problems associated with separation and filtration. It can be concluded that magnetic/biosilica/sodium alginate composites can be applied as an efficient adsorbent for removing Pb^{2+} from the aqueous environment of the industrial processes.

Acknowledgments

We acknowledge the financial and spiritual support of the University of Medical Sciences, Iran, for the research project with code 24659.

References

1. Pawar RR, Hong S-M, Jin KJ, Lee S-M. Iron-oxide modified sericite alginate beads: A sustainable adsorbent for the removal of As (V) and Pb (II) from aqueous solutions. J Mol Liq 2017; 240: 497-503.
2. Muhammad A. Albakri, Mahmoud M. Abdelnaby, Tawfik A. Saleh, Othman Charles S. Al Hamouz. New series of benzene-1, 3, 5-triamine based cross-linked polyamines and polyamine/CNT composites for lead ion removal from aqueous solutions. Chem Eng J 2018; 333: 76-84.
3. Tang J, He J, Xin X, Hu H, Liu T. Biosurfactants enhanced heavy metals removal from sludge in the electrokinetic treatment. Chem Eng J 2018;334: 2579-92.
4. Mahmoud M, Hassan S, Kamel A, Elserw M. Development of microwave-assisted functionalized nanosilicas for instantaneous removal of heavy metals. Powder Technol 2018;326: 13.
5. Shi Z, Xu C, Guan H, Li L, Fan L, Wang Y, et al. Magnetic Metal Organic Frameworks (MOFs) Composite for Removal of Lead and Malachite Green in Wastewater. Colloids Surf A Physicochem Eng Asp 2018; 539:328-390.
6. Burakov AE, Galunin EV, Burakova IV, Kucherova AE, Agarwal S, Tkachev AG, et al. Adsorption of heavy metals on conventional and nanostructured materials for wastewater treatment purposes: A review. Ecotoxicol Environ Saf 2018; 148: 702-12.
7. Ghaemi N, Zereshki S, Heidari S. Removal of lead ions from water using PES-based nanocomposite membrane incorporated with polyaniline modified GO nanoparticles: Performance optimization by central composite design. Process Saf Environ Prot 2017;111: 475-90.
8. Kakavandi B, Kalantary RR, Jafari AJ, Nasseri S, Ameri A, Esrafili A, et al. Pb (II) adsorption onto a magnetic composite of activated carbon and superparamagnetic Fe_3O_4 nanoparticles: experimental and modeling study. Clean: Soil, Air, Water 2015;43(8): 1157-66.
9. Vilardi G, Di Palma L, Verdone N. Heavy metals adsorption by banana peels micro-powder: Equilibrium modeling by non-linear models. Chin J Chem Eng 2017; 26(3):455-464.
10. Verma R, Asthana A, Singh AK, Prasad S, Susan MABH. Novel glycine-functionalized magnetic nanoparticles entrapped calcium alginate beads for effective removal of lead. Microchem J 2017; 130: 168-78.
11. Lam B, Déon S, Morin-Crini N, Crini G, Fievet P. Polymer-enhanced ultrafiltration for heavy metal removal: Influence of chitosan and carboxymethyl cellulose on filtration performances. J Clean Prod 2018; 171: 927-33.
12. Ayawanna J, Sato K. Photoelectrodeposition effect of lanthanum oxide-modified ceria particles on the removal of lead (II) ions from water. Catal Today 2017. (Article in Press)
13. Pal P, Syed SS, Banat F. Gelatin-bentonite composite as reusable adsorbent for the removal of lead from aqueous solutions: Kinetic and equilibrium studies. J Water Process Eng 2017;20: 40-50.
14. Mousa NE, Simonescu CM, Pătescu R-E, Onose C, Tardei C, Culiță DC, et al. Pb^{2+} removal from aqueous synthetic solutions by calcium alginate and chitosan coated calcium alginate. React Funct Polym 2016; 109: 137-50.
15. Yegane badi M, Azari A, Esrafili A, Ahmadi E, Gholami M. Performance evaluation of magnetized multiwall carbon nanotubes by iron

oxide nanoparticles in removing fluoride from aqueous solution. J Mazandaran Univ Med Sci 2015;25(124): 128-42.
16. Abdellaoui Y, Olguín MT, Abatal M, Ali B, Méndez SED, Santiago AA. Comparison of the divalent heavy metals (Pb, Cu and Cd) adsorption behavior by montmorillonite-KSF and their calcium-and sodium-forms. Superlattices Microstruct 2017. (Article in Press)
17. Yi X, He J, Guo Y, Han Z, Yang M, Jin J, et al. Encapsulating Fe_3O_4 into calcium alginate coated chitosan hydrochloride hydrogel beads for removal of Cu (II) and U (VI) from aqueous solutions. Ecotoxicol Environ Saf 2018; 147: 699-707.
18. Liu J, Zhang Y, Chen D, Yang T, Chen Z, Pan S, et al. Facile synthesis of high-magnetization γ-Fe_2O_3/alginate/silica microspheres for isolation of plasma DNA. Colloids Surf A Physicochem Eng Asp 2009; 341(1-3): 33-9.
19. Hu Z-H, Omer AM, Ouyang Xk, Yu D. Fabrication of carboxylated cellulose nanocrystal/sodium alginate hydrogel beads for adsorption of Pb (II) from aqueous solution. Int J Biol Macromol 2018; 108: 149-57.
20. Facchi DP, Cazetta AL, Canesin EA, Almeida VC, Bonafé EG, Kipper MJ, et al. New magnetic chitosan/alginate/Fe_3O_4@ SiO_2 hydrogel composites applied for removal of Pb (II) ions from aqueous systems. Chem Eng J 2017; 337:595-608.
21. Zhao X, Li J, Feng Y, Yu G, Zhou Q, He F, et al. Self-aggregation behavior of hydrophobic sodium alginate derivatives in aqueous solution and their application in the nanoencapsulation of acetamiprid. Int J Biol Macromol 2018; 106: 418-24.
22. Al-Ghouti M, Khraisheh M, Ahmad M, Allen S. Thermodynamic behaviour and the effect of temperature on the removal of dyes from aqueous solution using modified diatomite: a kinetic study. J Colloid Interface Sci 2005;287(1): 6-13.
23. Yuan P, Liu D, Fan M, Yang D, Zhu R, Ge F, et al. Removal of hexavalent chromium [Cr (VI)] from aqueous solutions by the diatomite-supported/unsupported magnetic nanoparticles. J Hazard Mater 2010; 173(1-3): 614-21.
24. Karaman S, Karaipekli A, Sarı A, Bicer A. Polyethylene glycol (PEG)/diatomite composite as a novel form-stable phase change material for thermal energy storage. Sol Energy Mater Sol Cells 2011;95(7): 1647-53.
25. Farooghi A, Sayadi MH, Rezaei MR, Allahresani A. An efficient removal of lead from aqueous solutions using $FeNi_3$@ SiO_2 magnetic nanocomposite. Surfaces and Interfaces 2018;10: 58-64.
26. Sun Z, Yao G, Liu M, Zheng S. In situ synthesis of magnetic $MnFe_2O_4$/diatomite nanocomposite adsorbent and its efficient removal of cationic dyes. J Taiwan Inst Chem Eng 2017;71: 501-9.
27. Vojoudi H, Badiei A, Bahar S, Ziarani GM, Faridbod F, Ganjali MR. A new nano-sorbent for fast and efficient removal of heavy metals from aqueous solutions based on modification of magnetic mesoporous silica nanospheres. J Magn Magn Mater 2017; 441:193-203.
28. Lou Z, Zhou Z, Zhang W, Zhang X, Hu X, Liu P, et al. Magnetized bentonite by Fe_3O_4 nanoparticles treated as adsorbent for methylene blue removal from aqueous solution: synthesis, characterization, mechanism, kinetics and regeneration. J Taiwan Inst Chem Eng 2015; 49: 199-205.
29. Soltani RDC, Khataee A, Safari M, Joo S. Preparation of bio-silica/chitosan nanocomposite for adsorption of a textile dye in aqueous solutions. Int Biodeterior Biodegradation 2013;85: 383-91.
30. Hossaini H, Moussavi G, Farrokhi M. The investigation of the LED-activated FeFNS-TiO_2 nanocatalyst for photocatalytic degradation and mineralization of organophosphate pesticides in water. Water Res 2014;59: 130-44.
31. Khaniabadi YO, Heydari R, Nourmoradi H, Basiri H, Basiri H. Low-cost sorbent for the removal of aniline and methyl orange from liquid-phase: Aloe Vera leaves wastes. J Taiwan Inst Chem Eng 2016;68: 90-8.
32. Yahong Z, Zhenhua X, Ximing W, Li W, Aiqin W. Adsorption of congo red onto lignocellulose/montmorillonite nanocomposite. J Wuhan Univ Technol Mater Sci Ed 2012;27: 931-8.
33. Shi W, Guo F, Wang H, Liu C, Fu Y, Yuan S, et al. Carbon dots decorated magnetic $ZnFe_2O_4$ nanoparticles with enhanced adsorption capacity for the removal of dye from aqueous solution. App Surf Sci 2018; 433: 790-7.
34. Mouni L, Belkhiri L, Bollinger J-C, Bouzaza A, Assadi A, Tirri A, et al. Removal of Methylene Blue from aqueous solutions by adsorption on Kaolin: Kinetic and equilibrium studies. Appl Clay Sci 2018;153: 38-45.

35. Yang Q, Wang Y, Wang J, Liu F, Hu N, Pei H, et al. High Effective Adsorption/Removal of Illegal Food Dyes from Contaminated Aqueous Solution by Zr-MOFs (UiO-67). Food Chem 2018;254:241-248.
36. Zakaria ND, Yusof NA, Haron J, Abdullah AH. Synthesis and evaluation of a molecularly imprinted polymer for 2, 4-dinitrophenol. Int J Mol Sci 2009; 10(1): 354-65.
37. Martins AC, Pezoti O, Cazetta AL, Bedin KC, Yamazaki DAS, Bandoch GFG, et al. Removal of tetracycline by NaOH-activated carbon produced from macadamia nut shells: Kinetic and equilibrium studies. Chem Eng J 2015; 260: 291-9.
38. Gao Y, Li Y, Zhang L, Huang H, Hu J, Shah SM, et al. Adsorption and removal of tetracycline antibiotics from aqueous solution by graphene oxide. J Colloid Interface Sci 2012;368(1): 540-6.
39. Soltanian M, Pirsaheb M, Almasi A, Masoud M, SHarafi K, Soltanian S. Kinetic and isotherm study of methylene blue dye adsorption by powdered natural pumice from the aquatic environment. The Journal of Toloo-e-behdasht 2015;14(5): 50-63.
40. Boparai HK, Joseph M, O'Carroll DM. Kinetics and thermodynamics of cadmium ion removal by adsorption onto nano zerovalent iron particles. J Hazard Mater 2011;186(1): 458-65.
41. Foo KY, Hameed BH. Insights into the modeling of adsorption isotherm systems. Chem Eng J 2010; 156(1): 2-10.
42. Nourmoradi H, Zabihollahi S, Pourzamani H. Removal of a common textile dye, navy blue (NB), from aqueous solutions by combined process of coagulation–flocculation followed by adsorption. Desalination Water Treat 2016; 57(11): 5200-11.
43. Ofomaja AE. Intraparticle diffusion process for lead (II) biosorption onto mansonia wood sawdust. Bioresour Technol 2010;101(15): 5868-76.
44. Zawani Z, Chuah AL, Choong T. Equilibrium, kinetics and thermodynamic studies: adsorption of Remazol Black 5 on the palm kernel shell activated carbon. European Journal of Scientific Research 2009;37: 67-76.
45. Sundarrajan P, Eswaran P, Marimuthu A, Subhadra LB, Kannaiyan P. One pot synthesis and characterization of alginate stabilized semiconductor nanoparticles. Bull Korean Chem Soc 2012;45(43): 3218-24.
46. Pezeshkpour S, Salamatinia B, Horri BA. Synthesis and characterization of nanocrystalline NiO-GDC via sodium alginate-mediated ionic sol-gel method. Ceram Int 2018;44(3): 3201-10.
47. Aprilliza M. Characterization and properties of sodium alginate from brown algae used as an ecofriendly superabsorbent. IOP Conference Series: Materials Science and Engineering; 2017: IOP Publishing.
48. Kulig D, Zimoch-Korzycka A, Jarmoluk A, Marycz K. Study on alginate–chitosan complex formed with different polymers ratio. Polymers 2016;8(5): 167.
49. Stuart B. Infrared Spectroscopy: Fundamentals and Applications. John Wiley & Sons; 2004. 208 p.
50. Badii K, Ardejani FD, Saberi MA, Limaee NY. Adsorption of Acid blue 25 dye on diatomite in aqueous solutions. Ind J Chem tecnol 2010; 17:7-16.
51. Wang L, Zhang J, Wang A. Removal of methylene blue from aqueous solution using chitosan-g-poly (acrylic acid)/montmorillonite superadsorbent nanocomposite. Colloids Surf A Physicochem Eng Asp 2008; 322(1-3): 47-53.
52. Wang Y, Feng Y, Zhang X-F, Zhang X, Jiang J, Yao J. Alginate-based attapulgite foams as efficient and recyclable adsorbents for the removal of heavy metals. J Colloid Interface Sci 2018;514: 190-8.
53. Culita DC, Simonescu CM, Patescu R-E, Dragne M, Stanica N, Oprea O. o-Vanillin functionalized mesoporous silica – coated magnetite nanoparticles for efficient removal of Pb(II) from water. J Solid State Chem 2016;238: 311-20.
54. Saha S, Basu H, Singhal RK, Pimple MV. Titania coated silica microsphere functionalized with potassium ferrocyanide impregnated in calcium alginate for efficient removal of Cs from aquatic environment. J Environ Chem Eng 2017;5: 5187-95.
55. Huang Y, Wang Z. Preparation of composite aerogels based on sodium alginate, and its application in removal of Pb^{2+} and Cu^{2+} from water. Int J Biol Macromol 2018;107: 741-7.
56. Yari M, Norouzi M, Mahvi AH, Rajabi M, Yari A, Moradi O, et al. Removal of Pb (II) ion from aqueous solution by graphene oxide and functionalized graphene oxide-thiol: effect of cysteamine concentration on the bonding constant. Desalination Water Treat 2016;57: 11195-210.
57. Badi MY, Azari A, Pasalari H, Esrafili A, Farzadkia M. Modification of activated carbon with magnetic Fe_3O_4 nanoparticle composite for removal of ceftriaxone from aquatic solutions. J Mol Liq 2018; 261:146-154.
58. Wu J, Wang X-B, Zeng RJ. Reactivity enhancement of iron sulfide nanoparticles stabilized by sodium alginate: Taking Cr (VI)

removal as an example. J Hazardous Mater 2017;333: 275-84.
59. Hashemi F, Godini H, Shams Khorramabadi G, Mansouri L. Assessing Performance of Walnut Green Hull Adsorbent in Removal of Phenol from Aqueous Solutions. Iran J Health Environ 2014; 7 (2) :265-276
60. Onyango MS, Masukume M, Ochieng A, Otieno F. Functionalised natural zeolite and its potential for treating drinking water containing excess amount of nitrate. Water SA 2010;36(5): 655-62.
61. Shi L-n, Zhang X, Chen Z-l. Removal of chromium (VI) from wastewater using bentonite-supported nanoscale zero-valent iron. Water Res 2011;45(2): 886-92.
62. Acharya J, Sahu J, Mohanty C, Meikap B. Removal of lead (II) from wastewater by activated carbon developed from Tamarind wood by zinc chloride activation. Chem Eng J 2009;149(1-3) 249-62.
63. Allen S, Mckay G, Porter JF. Adsorption isotherm models for basic dye adsorption by peat in single and binary component systems. J Colloid Interface Sci 2004;280(2): 322-33.
64. Dada A, Olalekan A, Olatunya A, Dada O. Langmuir, Freundlich, Temkin and Dubinin–Radushkevich isotherms studies of equilibrium sorption of Zn^{2+} unto phosphoric acid modified rice husk. IOSR J App Chem 2012;3(1): 38-45.
65. Zanin E, Scapinello J, de Oliveira M, Rambo CL, Franscescon F, Freitas L, et al. Adsorption of heavy metals from wastewater graphic industry using clinoptilolite zeolite as adsorbent. Process Saf Environ Prot 2017;105: 194-200.
66. Nourmoradi H, Avazpour M, Ghasemian N, Heidari M, Moradnejadi K, Khodarahmi F, et al. Surfactant modified montmorillonite as a low cost adsorbent for 4-chlorophenol: Equilibrium, kinetic and thermodynamic study. J Taiwan Inst Chem Eng 2016;59: 244-51.
67. Shaker MA, Yakout AA. Optimization, isotherm, kinetic and thermodynamic studies of Pb (II) ions adsorption onto N-maleated chitosan-immobilized TiO_2 nanoparticles from aqueous media. Spectrochim Acta A Mol Biomol Spectrosc 2016;154: 145-56.